Journal of Rock Mechanics and Geotechnical Engineering 18 (2026) 3333–3347

Contents lists available at ScienceDirect

Journal of Rock Mechanics and Geotechnical Engineering

journal homepage: www.jrmge.cn

Full Length Article

Three-dimensional time-dependent fracturing model for hard rock involving stress-induced anisotropic cracks

Chen Fan [a,b], Xia-Ting Feng [a,b,*], Jun Zhao [a,b], Chengxiang Yang [a,b], Mengfei Jiang [a,b]

[a] State Key Laboratory of Intelligent Deep Metal Mining and Equipment, Northeastern University, Shenyang, 110819, China
[b] Key Laboratory of Liaoning Province on Deep Engineering and Intelligent Technology, Northeastern University, Shenyang, 110819, China

ARTICLE INFO

Article history:
Received 1 March 2025
Received in revised form
3 June 2025
Accepted 10 July 2025
Available online 23 December 2025

Keywords:
Three-dimensional (3D) time-dependent model
Continuous fracturing process
Microcrack development
Time-dependent anisotropic fracturing
True triaxial stress

ABSTRACT

The time-dependent failure of surrounding rock in deep engineering is essentially controlled by the evolution of microcracks, with the pre-existing fracturing state induced by excavation playing a crucial role in the subsequent time-dependent fracturing process. From the perspective of microcrack development, it is a continuous, dynamic process. Therefore, taking the microcrack propagation process as the fundamental principle, this paper proposes a novel three-dimensional (3D) time-dependent model for hard rock that can depict the entire fracturing process within a unified theoretical framework. This developed model discards the traditional tri-modal partition method based on deformation, and instead adopts an analysis approach centred on time-dependent tensile and shear fracturing. The results show that the time-dependent deformation of hard rock is the macroscopic manifestation of the progressive evolution of microcracks over time. Under true triaxial stress, the growth tendency of cracks in hard rock is orientation-dependent throughout the entire loading process. This developed model provides a mechanical explanation for key time-dependent fracture characteristics observed in true triaxial creep tests, including the anisotropy of time-dependent deformation and the preferred orientation of macroscopic failure plane, and provides a novel framework for elucidating the time-dependent failure process of hard rock.

1. Introduction

With the increasing depth of underground engineering, the frequency of time-dependent surrounding rock failures has increased, significantly affecting the long-term stability. High in situ stress has been one of the primary challenges in deep engineering, making the surrounding rock exhibit pronounced time-dependent characteristics. In previous engineering construction, various types of time-delayed surrounding rock failures have been reported, including time-delayed rockbursts (Feng et al., 2019a; He et al., 2023; Jiang et al., 2024), time-delayed large deformations (Kontogianni and Stiros, 2005), and time-delayed spalling (Fan et al., 2023). Under high deviatoric stress, fracturing events continued to occur in the surrounding rock after excavation, and time-delayed failures evolved with time, showing noticeable spatial-temporal lag characteristics and posing a significant threat to workers' security. Therefore, it is of great importance to investigate the time-dependent failure process of hard rock under true triaxial stress.

As a bridge between mechanism research and engineering applications, theoretical models that describe the time-dependent failure process of hard rock have been extensively investigated. Based on the differences in theoretical frameworks, time-dependent constitutive models could be divided into several categories, including empirical models (Okubo et al., 2008; Wei et al., 2021), element-combination models (Yang et al., 2014; Zhao et al., 2017), viscous-elastic-plastic models (Shao et al., 2003; Zhao et al., 2016), damage models (Tran-Manh et al., 2016; Xu et al., 2018), and microcrack models (Shao et al., 2006; Brantut et al., 2012; Yang et al., 2021; Sisodiya and Zhang, 2022; Li et al., 2024). Methodologically, empirical rheological models, element-combination rheological models, and viscous-elastic-plastic rheological models all belong to phenomenological models. These models

* Corresponding author. State Key Laboratory of Intelligent Deep Metal Mining and Equipment, Northeastern University, Shenyang, 110819, China.
E-mail address: fengxiating@mail.neu.edu.cn (X.-T. Feng).

Peer review under responsibility of Institute of Rock and Soil Mechanics, Chinese Academy of Sciences.

https://doi.org/10.1016/j.jrmge.2025.07.042

mainly simulate the variation of creep deformation over time based on the macroscopic rheological phenomenon, without delving into the intrinsic fracture mechanism in hard rock. The damage rheological models also belong to the phenomenological model to some extent. By introducing a macroscopic damage field into the constitutive relationship of hard rock, it avoids the complexity of fracture evolution characteristics on the microscopic or mesoscopic level. Although this facilitates the model development, it comes at the expense of sacrificing the physical foundation of rheological models. As for the microcrack rheological model, the time-dependent failure process of hard rock is primarily attributed to the subcritical propagation of cracks, which is often integrated with the wing crack propagation model for theoretical analysis (Brantut et al., 2012; Yang et al., 2021; Bernabé and Pec, 2022; Li et al., 2024). The focus of such models lies in describing the subcritical propagation and interaction of cracks at the microscopic scale, as well as their influence on the macroscopic mechanical properties of rocks. Despite its robust physical foundation, this analytical method faces challenges in addressing cross-scale issues when linking microscopic fracturing behaviors with macroscopic degradation of mechanical properties. Consequently, most models quantify the effects of time-dependent crack evolution either through energy analysis (Brantut et al., 2012) or by simplifying them as macroscopic damage factors (Bikong et al., 2015; Li et al., 2020, 2024; Yang et al., 2021). Although these models have demonstrated good performance in characterizing the time-dependent deformation of hard rock, most of them fail to adequately explain key fracturing characteristics observed during the rock failure, such as time-dependent anisotropic fracturing and the formation of a macroscopic failure plane. Moreover, existing models predominantly concentrate on time-dependent axial deformation in the σ_1 direction, lacking a systematic theoretical framework for understanding the anisotropic time-dependent deformation process under true triaxial stress conditions. These limitations restrict their ability to provide guidance for time-dependent failures in deep engineering.

During the development of time-delayed disasters, the failure process is not solely dictated by time-dependent fracturing under high geostress, but also relies on the pre-existing damage during excavation. This pre-existing damage could be regarded as the inception of the time-delayed disaster evolution. As excavation progresses, randomly distributed microdefects (e.g. cracks or mineral structural defects) in the surrounding rock gradually evolve under increasing deviatoric stress (Fan et al., 2025a), causing irreversible damage in the rock's microstructure. In hard rocks, this damage is irreversible, and the ultimate failure results from the continuous accumulation of internal damage. Consequently, when assessing the long-term stability of surrounding rock in deep engineering, the pre-existing damage caused by excavation cannot be disregarded. In addition, the fracturing state of hard rock during the time-dependent loading stage is inherently influenced by its prior loading history. Variations in loading history would lead to different fracturing states at any given moment. However, in previous rheological models, the pre-existing damage is often neglected or oversimplified, which is prone to misestimating the time-dependent failure process of hard rock under high geostress. Hence, the assessment of the fracturing process during the time-dependent loading stage should be based on the preceding fracturing history. A rheological model based on the continuous fracturing process will help to portray the fracturing state of the surrounding rock at different times after excavation, facilitating a more precise prediction of the time-dependent failure process.

Essentially, the failure process of hard rock is governed by the continuous propagation and coalescence of internal cracks, irrespective of whether the failure is instantaneous or time-dependent. Although the entire loading–fracturing process could be distinguished into different loading stages (e.g. instantaneous loading stage, time-dependent loading stage, and others), the propagation of microcracks throughout the rock failure process is continuous. Therefore, taking the propagation process of microcracks in different orientations as the fundamental principle, this study proposes a novel time-dependent fracturing model and offers new insights into the mechanisms of the progressive rock failure process.

2. Anisotropic fracture evolution during the instantaneous loading stage

To describe the anisotropic fracturing state of hard rock under instantaneous loading, Fan et al. (2025b) proposed a competitive anisotropic fracturing model (CAFM) based on the competitive growth of cracks with different orientations. In CAFM, numerous randomly dispersed microdefects in hard rock are assumed to be randomly oriented microcracks. The inelastic deformation of hard rock can be decomposed into two parts: open-tensile microcrack development and penetrative-shear microcrack development. Therefore, the total strain of hard rock under true triaxial stress could be regarded as the superposition of elastic deformation caused by stress acting on the undamaged matrix and the discontinuous displacement caused by microcracks, which could be expressed as follows:

$$\varepsilon_{ij} = C^{\mathrm{e}}_{ijkl}\sigma_{kl} + \left(C^{\mathrm{ct}}_{ijkl} + C^{\mathrm{pt}}_{ijkl}\right)\sigma_{\mathrm{T}kl} + \left(C^{\mathrm{cs}}_{ijkl} + C^{\mathrm{ps}}_{ijkl}\right)\sigma_{kl} \tag{1}$$

where ε_{ij} and σ_{ij} are the macroscopic strain and stress, respectively; $\sigma_{\mathrm{T}ij}$ is the compression-induced tensile stress, with the nonvanishing components including $\sigma_{\mathrm{T}22} = \nu(\sigma_1 + \sigma_3) - \sigma_2$ and $\sigma_{\mathrm{T}33} = \nu(\sigma_1 + \sigma_2) - \sigma_3$, in which ν is the Poisson's ratio; C^{e}_{ijkl} is the elastic compliance tensor of the undamaged rock matrix; C^{ct}_{ijkl} and C^{cs}_{ijkl} are the inelastic compliance tensors resulting from open-tensile crack propagation, corresponding to the contributions of open-tensile cracks and penetrative-shear cracks, respectively; and C^{pt}_{ijkl} and C^{ps}_{ijkl} are the inelastic compliance tensors resulting from crack coalescence, corresponding to the contributions of open-tensile cracks and penetrative-shear cracks respectively. The key parameters of crack growth in CAFM include tensile fracture toughness K_{IC}, shear fracture toughness K_{IIC}, and shear crack propagation parameters A_{s} and n.

In the instantaneous loading stage, the propagation of cracks is primarily attributed to the increase of deviatoric stress ($\sigma_1 - \sigma_3$). Upon transitioning to the time-dependent loading stage, the stress state becomes constant, meaning that the crack growth mode driven by stress increase in CAFM is no longer applicable. However, the failure process of hard rock is still essentially controlled by the evolution of microcrack ensembles. Despite variations in crack propagation mechanisms across different loading stages, the CAFM analysis framework remains valid as it was developed based on crack propagation in various orientations. Furthermore, from the perspective of microcrack development, the progressive rock failure process is continuous and irreversible. When analyzing the time-dependent fracturing process of hard rock, the irreversible damage incurred in the instantaneous stage cannot be ignored. Based on the theoretical framework provided by CAFM, the entire fracturing process, including the instantaneous and the time-dependent loading stages, can be subjected to continuous and systematic analysis.

3. Anisotropic fracture evolution during the time-dependent loading stage

Under persistent external loading, the creep failure of hard rock could be regarded as the gradual deviation of the stress–rock system from equilibrium over time, which is primarily controlled by the subcritical propagation of microcracks. The failure process of hard rock relies on the collective evolution and interaction of microdefects inside. Under the influence of applied stress, the initially randomly distributed microdefects tend to undergo directional development. Thus, starting from the initial fracturing state in hard rock, a multiscale anisotropic rheological model will be established by focusing on the collective development process of microcracks, which aims to elucidate the sustained fracturing process over time.

The inception of the time-dependent fracturing process is the fracturing state of hard rock after the instantaneous loading stage. In the instantaneous loading stage, the initial fracturing state of hard rock could be analyzed with the CAFM. Therefore, the current task is exploring the rheological evolution of hard rock from the mesoscopic fracturing mechanism. The propagation and coalescence of microcracks constitute the predominant failure mechanism in hard rock, which also applies to the time-dependent failure process. During the instantaneous loading stage, the system, consisting of external stress and hard rock with internal cracks, forms a dynamic equilibrium, and microcracks would extend once the driving force is sufficient to overcome the rock's fracture resistance. As the transitions to the time-dependent loading stage occur, microcracks continue to propagate steadily in a quasi-static state, known as subcritical crack growth. Stress corrosion is widely considered the dominant mechanism for crack growth in this stage.

Derived from the CAFM, the analysis of time-dependent failure process is also divided into the subcritical propagation of open-tensile cracks and the subcritical propagation of penetrative-shear cracks, as shown in Fig. 1. Throughout the progressive failure process, microcracks in hard rock propagate and coalesce over time under high deviatoric stress, leading to the development of inelastic strain and cumulative fracturing.

In view of the variable orientations of local microcracks, it involves the transformation between the local and the global coordinate systems, as depicted in Fig. 1b. The coordinate transformation matrix between the global and the local coordinate systems could be expressed as (Fan et al., 2025b):

$$T_{ij}^{(k)}=\begin{bmatrix}\cos\theta & \sin\theta\cos\varphi & \sin\theta\sin\varphi\\ -\sin\theta & \cos\theta\cos\varphi & \cos\theta\sin\varphi\\ 0 & -\sin\varphi & \cos\varphi\end{bmatrix} \tag{2}$$

where (θ, φ) is the kth crack orientation, indicating the dip angle and dip, respectively. Particularly, since open-tensile cracks are simplified to propagate along the σ_1-direction, the dip angle of open-tensile cracks is $\theta = 90^\circ$.

Stress corrosion is widely considered the dominant mechanism for crack growth in hard rock during the time-dependent loading stage (Anderson and Grew, 1977), and the crack propagation rate is dynamically controlled by the stress intensity factor at the crack tip (Atkinson, 1987). Subsequently, the subcritical propagation of open-tensile and penetrative-shear cracks will be analyzed separately. For open-tensile cracks, new crack surfaces would be generated over time after entering the time-dependent loading stage. The subcritical crack propagation rate and total length of the kth open-tensile crack at time t could be assumed as

$$\dot{a}_{(k)}(t)=A_{\mathrm{a}}\left(\frac{K_{\mathrm{I}}^{\mathrm{ct}(k)}(t)}{K_{\mathrm{Isc}}}\right)^{n_{\mathrm{a}}} \tag{3}$$

$$a_{(k)}(t)=a_{(k)}(t-\Delta t)+\dot{a}_{(k)}(t-\Delta t)\Delta t \tag{4}$$

where $a_{(k)}(t)$ and $\dot{a}_{(k)}(t)$ are the crack radius and the subcritical propagation rate of the kth tensile crack with orientation ($\theta = \pi/2$, φ) at time t during the long-term loading stage, respectively; the initial radius of the kth open-tensile crack when entering the time-dependent loading stage, namely $a_{(k)}(0)$, corresponds to the final state in the instantaneous loading stage; A_{a} and n_{a} are the subcritical tensile crack growth parameters during the long-term loading stage; and K_{Isc} is the subcritical fracture threshold of open-tensile cracks. $K_{\mathrm{I}}^{\mathrm{ct}(k)}(t)$ is the stress intensity factor of the kth tensile crack with orientation ($\theta = \pi/2$, φ) at time t, and could be written as (Fan et al., 2025b):

$$K_{\mathrm{I}}^{\mathrm{ct}(k)}(t)=\tau_{\mathrm{es}}^{\mathrm{cs}(k)}S_{\mathrm{cs}(k)}\cos\theta\Big/\left[\pi a_{(k)}(t)\right]^{3/2}-2\sigma_{11}^{\mathrm{cs}(k)}\sqrt{a_{(k)}(t)/\pi} \tag{5}$$

$$\tau_{\mathrm{es}}^{\mathrm{cs}(k)}=\sqrt{\left(\sigma_{12}^{\mathrm{cs}(k)}\right)^2+\left(\sigma_{13}^{\mathrm{cs}(k)}\right)^2}-\mu\sigma_{11}^{\mathrm{cs}(k)} \tag{6}$$

where $\tau_{\mathrm{es}}^{\mathrm{cs}(k)}$ is the driving shear stress parallel to the kth shear crack surface; μ is the frictional coefficient of the shear crack interface, which is assumed to be related to the internal friction angle in the strength criterion; $S_{\mathrm{cs}(k)}$ is the surface area of the shear crack; $\sigma_{11}^{\mathrm{ct}(k)}$ denotes the inhibitive normal stress on the open-tensile crack surfaces provided by the far-field applied stress; and $\sigma_{ij}^{\mathrm{c}(k)}$ (including $\sigma_{ij}^{\mathrm{cs}(k)}$ and $\sigma_{ij}^{\mathrm{ct}(k)}$), expressed as $\sigma_{ij}^{\mathrm{c}(k)} = T_{im}^{(k)}T_{jn}^{(k)}\sigma_{mn}$, is the stress around microcracks in the local coordinate provided by far-field stress applied and only the stress components $\sigma_{1j}^{\mathrm{c}(k)}$ on the crack surface are assumed to promote microcrack propagation.

During the time-dependent loading stage, the crack length $a_{(k)}(t+\Delta t)$ at time $t + \Delta t$ was considered to be directly related to the fracture state at time t. Thus, a simple explicit method was adopted to calculate the crack length, as shown in Eq. (4). The accuracy is sufficient when the time interval Δt is suitable. For open-tensile cracks, the initial value $a_{(k)}(0)$ when entering the time-dependent loading stage should be the crack radius $a_{\mathrm{in}(k)}$ in the instantaneous loading stage, which could be written as

$$a_{(k)}(0)=a_{in(k)} \tag{7}$$

Consequently, combining Eq. (4), the radius increase of the corresponding shear crack at time t during the time-dependent loading stage could be expressed as (Fan et al., 2025b):

$$\Delta l_{(k)}(t)=\frac{16(1-\nu^2)}{2\pi E\cos\theta}\sigma_{\mathrm{ET}}^{\mathrm{ct}(k)}a_{(k)}(t) \tag{8}$$

where E is the elastic modulus. $\Delta l_{(k)}(t)$ is the radius increase of the kth shear crack contributed by tensile crack propagation at time t, which includes the radius increment ($\Delta l_{\mathrm{in}(k)}$) during the instant loading stage. $\sigma_{\mathrm{ET}}^{\mathrm{ct}(k)}$ denotes the macroscopic compression-induced tensile stress on the kth tensile crack surface, which is

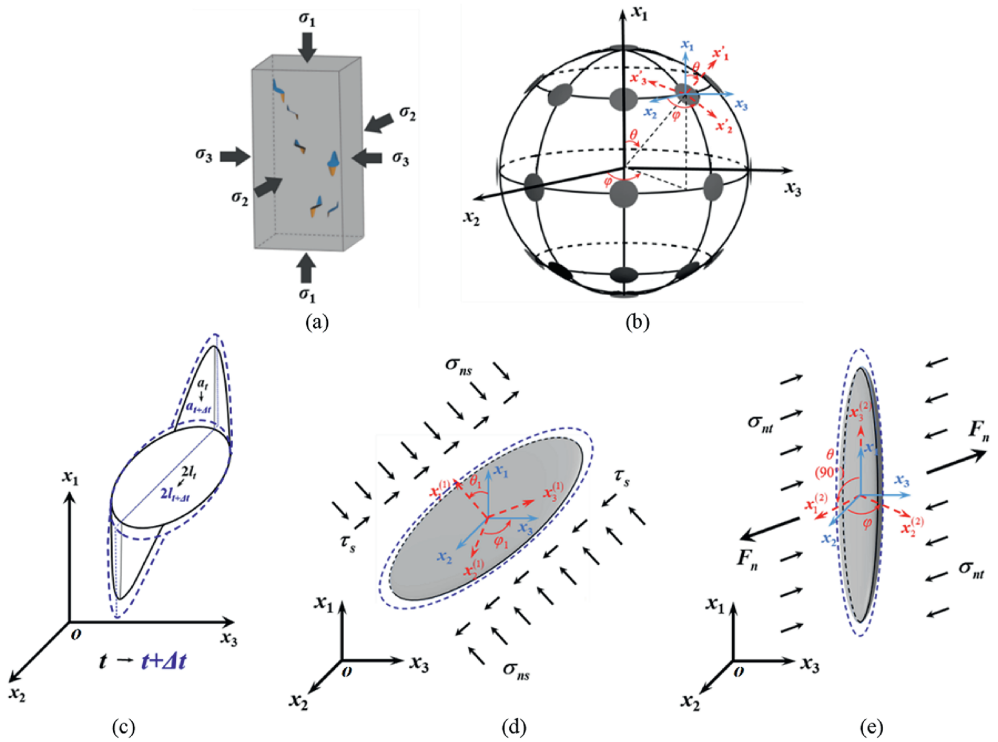

Fig. 1. Microcrack growth in time-dependent anisotropic fracturing model: (a) Randomly dispersed microdefects in hard rock (Fan et al., 2025b); (b) Randomly oriented penny-shaped microcracks simplified from dispersed microdefects; (c) Three-dimensional (3D) crack propagation over time under true triaxial stress; (d) Evolution of penetrative-shear crack with time under stress; and (e) Evolution of open-tensile crack with time under stress. $ox_1x_2x_3$ is the global coordinate system, $ox_1^{(1)}x_2^{(1)}x_3^{(1)}$ is the local coordinate system for the shear crack, and $ox_1^{(2)}x_2^{(2)}x_3^{(2)}$ is the local coordinate system associated with the corresponding tensile crack.

expressed as $\sigma_{\mathrm{ET}}^{\mathrm{ct}(k)} = \sigma_{\mathrm{T22}}\cos^2\varphi + \sigma_{\mathrm{T33}}\sin^2\varphi$.

Incorporating the propagation of oriented cracks over time, the nonzero components of the time-dependent inelastic compliance tensors in the local coordinate could be written as follows (Horii and Nemat-Nasser, 1983; Krajcinovic and Fanella, 1986):

$$C'^{\mathrm{ct}(k)}_{1111}(t) = \frac{16(1-\nu^2)}{3E}a^3_{(k)}(t) \tag{9}$$

$$\left.\begin{aligned} C'^{\mathrm{cs}(k)}_{1212}(t) = C'^{\mathrm{cs}(k)}_{1221}(t) = C'^{\mathrm{cs}(k)}_{2121}(t) = C'^{\mathrm{cs}(k)}_{2112}(t) = \frac{8(1-\nu^2)}{3E(2-\nu)}l^3_{(k)}(t) \\ C'^{\mathrm{cs}(k)}_{1313}(t) = C'^{\mathrm{cs}(k)}_{1331}(t) = C'^{\mathrm{cs}(k)}_{3131}(t) = C'^{\mathrm{cs}(k)}_{3113}(t) = \frac{8(1-\nu^2)}{3E(2-\nu)}l^3_{(k)}(t) \end{aligned}\right\} \tag{10}$$

where $C'^{\mathrm{ct}(k)}_{mnpq}(t)$ is the compliance tensor caused by an open-tensile crack in the local coordinate; $C'^{\mathrm{cs}(k)}_{mnpq}(t)$ is the compliance tensor caused by a single shear crack in the local coordinate; $a_{(k)}(t)$ is the radius of the kth open-tensile crack at time t; and $l_{(k)}(t)$ is the radius of the kth shear crack at time t, which could be expressed as $l_{(k)}(t) = l_0 + \Delta l_{(k)}(t)$, in which l_0 is the initial average radius of cracks in hard rock.

It is assumed that the orientations of microcracks are random, and the probability density of crack distribution should satisfy the normalization requirement. Thus, the overall time-dependent inelastic compliance tensor contributed by the tensile crack growth could be expressed as

$$C^{\mathrm{ct}}_{ijkl}(t) = \frac{N_{\mathrm{c}}}{2\pi}\int_0^{2\pi}\int_0^{\frac{\pi}{2}} C^{\mathrm{ct}(k)}_{ijkl}\left(a_{(k)}(t), l_{(k)}(t), \theta, \varphi\right)\langle\tau^{\mathrm{cs}(k)}_{\mathrm{es}}\rangle\sin\theta\mathrm{d}\theta\mathrm{d}\varphi \tag{11}$$

$$C^{\mathrm{cs}}_{ijkl}(t) = \frac{N_{\mathrm{c}}}{2\pi}\int_0^{2\pi}\int_0^{\frac{\pi}{2}} C^{\mathrm{cs}(k)}_{ijkl}\left(a_{(k)}(t), l_{(k)}(t), \theta, \varphi\right)\langle\tau^{\mathrm{cs}(k)}_{\mathrm{es}}\rangle\sin\theta\mathrm{d}\theta\mathrm{d}\varphi \tag{12}$$

where N_{c} is the microcrack number density. $C^{\mathrm{ct}(k)}_{ijkl}(t)$ and $C^{\mathrm{cs}(k)}_{ijkl}(t)$ are the time-dependent inelastic compliance tensors in the global coordinate corresponding to $C'^{\mathrm{ct}(k)}_{ijkl}(t)$ and $C'^{\mathrm{cs}(k)}_{ijkl}(t)$ in the local coordinate, respectively, which can be calculated as $C^{\mathrm{c}(k)}_{ijkl}(t) = T^{(k)}_{\alpha i}T^{(k)}_{\beta j}T^{(k)}_{\gamma k}T^{(k)}_{\delta l}C'^{\mathrm{c}(k)}_{\alpha\beta\gamma\delta}(t)$; and the bracket $\langle x\rangle$ here is a discriminant notation, meaning $\langle x\rangle = 1$ when $x > 0$ and $\langle x\rangle = 0$ when $x \le 0$.

During the progressive failure process, while open-tensile cracks propagate steadily over time, penetrative-shear cracks also evolve gradually based on the pre-existing fracturing state. Due to the crack tip shielding effect (Ritchie, 1988), penetrative-shear cracks are assumed to propagate from the tips of pre-existing cracks during the time-dependent loading stage. For the dynamic propagation of penetrative-shear cracks during the time-dependent loading stage, the subcritical crack propagation rate is also considered as a function of the applied stress intensity at the crack tip. Thus, the subcritical propagation rate and total length of the kth penetrative-shear crack at time t could be written as

$$\dot{l}_{\mathrm{p}(k)}(t)=A_{\mathrm{l}}\left(\frac{K_{\mathrm{II}}^{\mathrm{cs}(k)}(t)}{K_{\mathrm{IIsc}}}\right)^{n_{\mathrm{l}}} \tag{13}$$

$$l_{\mathrm{p}(k)}(t)=l_{\mathrm{p}(k)}(t-\Delta t)+\dot{l}_{\mathrm{p}(k)}(t-\Delta t)\Delta t \tag{14}$$

where $l_{\mathrm{p}(k)}(t)$ and $\dot{l}_{\mathrm{p}(k)}(t)$ are the length and subcritical growth rate of the kth penetrative-shear crack with orientation (θ, φ) at time t during the time-dependent loading stage, respectively; and A_{l} and n_{l} are the subcritical shear crack growth parameters. The predominant effect of crack growth in this part is the coalescence of cracks. For a penetrative-shear crack, the penetrating crack length $l_{\mathrm{p}(k)}(t)$ at time t during the time-dependent loading stage should also be based on the final penetrating crack length $l_{\mathrm{p\_in}(k)}$ after the instantaneous loading stage, which means $l_{\mathrm{p}(k)}(0)=l_{\mathrm{p\_in}(k)}$. K_{IIsc} is the subcritical fracture threshold of the shear crack. $K_{\mathrm{II}}^{\mathrm{cs}(k)}(t)$ is the stress intensity factor of the kth shear crack with orientation (θ, φ) at time t, which could be expressed as $K_{\mathrm{II}}^{\mathrm{cs}(k)}(t)=4\tau_{\mathrm{es}}^{\mathrm{cs}(k)}\sqrt{\pi l_{(k)}(t)}/[\pi(2-\nu)]$.

Thus, the inelastic compliance tensor arising from crack coalescence over time could be written as

$$C_{ijkl}^{\mathrm{pt}}(t)=\frac{N_{\mathrm{c}}}{2\pi}\int_0^{2\pi}\int_0^{\frac{\pi}{2}}\left[C_{ijkl}^{\mathrm{ct}(k)}\left(a_{(k)}(t),\left(1+c_{\mathrm{p}(k)}(t)\right)l_{(k)}(t),\theta,\varphi\right)-\left(1+c_{\mathrm{p}(k)}(t)\right)C_{ijkl}^{\mathrm{ct}(k)}\left(a_{(k)}(t),l_{(k)}(t),\theta,\varphi\right)\right]\langle K_{\mathrm{II}(k)}(t)-K_{\mathrm{IIsc}}\rangle\sin\theta\mathrm{d}\theta\mathrm{d}\varphi \tag{15}$$

$$C_{ijkl}^{\mathrm{ps}}(t)=\frac{N_{\mathrm{c}}}{2\pi}\int_0^{2\pi}\int_0^{\frac{\pi}{2}}\left[C_{ijkl}^{\mathrm{cs}(k)}\left(a_{(k)}(t),\left(1+c_{\mathrm{p}(k)}(t)\right)l_{(k)}(t),\theta,\varphi\right)-\left(1+c_{\mathrm{p}(k)}(t)\right)C_{ijkl}^{\mathrm{cs}(k)}\left(a_{(k)}(t),l_{(k)}(t),\theta,\varphi\right)\right]\langle K_{\mathrm{II}(k)}(t)-K_{\mathrm{IIsc}}\rangle\sin\theta\mathrm{d}\theta\mathrm{d}\varphi \tag{16}$$

where $c_{\mathrm{p}(k)}(t)$ is the time-dependent crack coalescence index for penetrative-shear cracks with orientation (θ, φ), which is expressed as $c_{\mathrm{p}(k)}(t)=l_{\mathrm{p}(k)}(t)/l_{\mathrm{b}(k)}$, in which $l_{\mathrm{b}(k)}$ is the length of the rock bridge.

Therefore, based on the continuous propagation process of microcracks in different orientations, the total strain of hard rock under true triaxial stress during the time-dependent loading stage could be expressed as Eq. (17), which has the same analytical form as that during the instantaneous loading stage shown in Eq. (1):

$$\varepsilon_{ij}=C_{ijkl}^{\mathrm{e}}\sigma_{kl}+\left(C_{ijkl}^{\mathrm{ct}}(t)+C_{ijkl}^{\mathrm{pt}}(t)\right)\sigma_{\mathrm{T}kl}+\left(C_{ijkl}^{\mathrm{cs}}(t)+C_{ijkl}^{\mathrm{ps}}(t)\right)\sigma_{kl} \tag{17}$$

where the deformation increase during the instantaneous loading process has also been included, as the time-dependent crack propagation depends on the pre-existing fracturing state in the instantaneous loading stage.

4. Model validation

4.1. Determination of model parameters

In the developed 3D time-dependent fracturing model, encompassing both the instantaneous and the time-dependent loading stages, the main parameters could be categorized into two types: instantaneous and time-dependent fracturing parameters.

Since the rock failure is a continuous fracturing process, the developed anisotropic rheological model only needs to superpose time-dependent fracturing parameters onto those in CAFM. For the instantaneous loading process, the instantaneous fracturing parameters include the microcrack number density N_{c}, the initial crack radius l_0, tensile fracture toughness K_{IC}, shear fracture toughness K_{IIC}, frictional coefficient μ, and the instantaneous shear crack growth parameters A_{s} and n. The identification methods of these instantaneous fracturing parameters have been introduced in CAFM (Fan et al., 2025b).

For the time-dependent fracturing process, the superimposed time-dependent fracturing parameters include the subcritical tensile crack growth threshold K_{Isc}, the subcritical shear crack growth threshold K_{IIsc}, the subcritical tensile crack growth parameters A_{a} and n_{a}, and the subcritical shear crack growth parameters A_{l} and n_{l}. For the subcritical crack propagation, the identification of these time-dependent fracturing parameters could refer to the experimental methods of the double torsion tests (Becker et al., 2011) and the short beam compression tests (Ko and Kemeny, 2011). However, due to the complicating factors (e.g. rock microstructure, environmental media, and temperature), the exact thresholds and propagation rate of subcritical cracks in hard rocks are difficult to experimentally measure. Hence, parameter inversion based on relevant experimental results may be a more feasible method to determine these time-dependent fracturing parameters.

4.2. Model validation

To validate the developed 3D time-dependent model, this study compares the simulation results with the true triaxial time-dependent tests of Beishan granite (Jiang et al., 2025). The instantaneous fracturing parameters are mainly based on those of Beishan granite used in Fan et al. (2025b). The time-dependent fracturing parameters were derived from inversion. In view of the relative independence of fracturing parameters in different loading stages, these parameters were also categorized into instantaneous and time-dependent fracturing parameters for inversion. During the inversion process, the problem is reformulated as an optimization problem of an objective function. Through multiple iterations, the trial values of unknown parameters are gradually adjusted until the desired parameter values are obtained. The computational algorithm for the time-dependent loading stage can refer to that for the instantaneous loading stage (Fan et al., 2025b).

As shown in Fig. 2, a true triaxial creep test was conducted at $\sigma_3=5$ MPa, $\sigma_2=30$ MPa, and $\sigma_1=259$ MPa, which lasted about 30 h. According to the elastic compression stage, the elastic modulus is $E=45{,}000$ MPa, and the Poisson's ratio is $\nu=0.38$. The average radius of initial microcracks in this granite sample is $l_0=1.1\times10^{-3}$ m. After entering the time-dependent loading stage, the subcritical propagation parameters for tensile and shear cracks are $A_{\mathrm{a}}=1.04\times10^{-4}$ m/h and $A_{\mathrm{l}}=9\times10^{-18}$ m/h. The remaining fracturing parameters adopted are listed in Table 1.

Fig. 3 compares the simulated stress–strain and strain–time curves of granite when $\sigma_3=5$ MPa, $\sigma_2=100$ MPa, and $\sigma_1=300$ MPa, which lasted about 380 h. According to the elastic compression stage, the elastic modulus is $E=54{,}000$ MPa, and the Poisson's ratio is $\nu=0.38$. The initial crack radius in this granite sample is $l_0=9.5\times10^{-4}$ m. After entering the time-dependent loading stage, the subcritical propagation parameters for tensile and shear cracks are $A_{\mathrm{a}}=9.92\times10^{-7}$ m/h and $A_{\mathrm{l}}=4.1\times10^{-20}$ m/h.

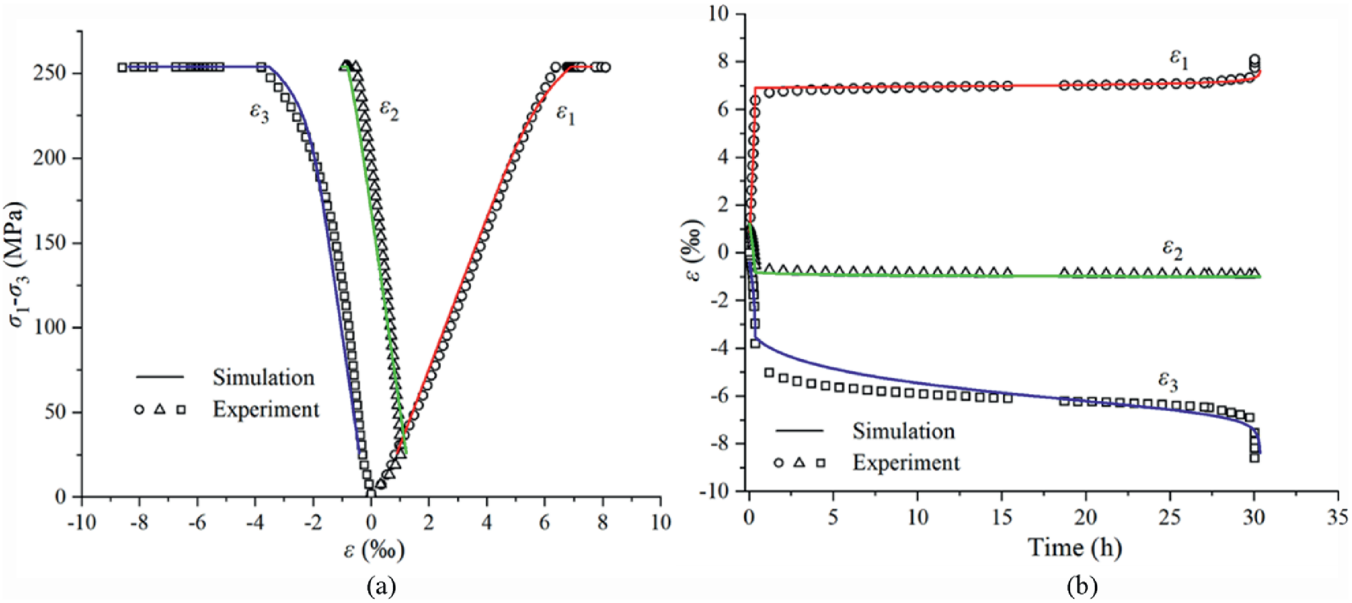

Fig. 2. Comparison between simulated and creep experimental results for granite when $\sigma_3 = 5$ MPa, $\sigma_2 = 30$ MPa, and $\sigma_1 = 259$ MPa: (a) Stress–strain curves; and (b) Strain–time curves.

Table 1
Fracturing parameters for Beishan granite.

Fracturing parameters	Value
Microcrack number density, N_c	$4 \times 10^6/m^3$
Angle of internal friction	38°
Fracture toughness of tensile cracks, K_{IC}	0.8 MPa $m^{1/2}$
Fracture toughness of shear cracks, K_{IIC}	1 MPa $m^{1/2}$
Instantaneous shear crack growth parameter, A_s	3×10^{-4} m/s
Instantaneous shear crack growth parameter, n	4
Subcritical tensile crack growth threshold, K_{Isc}	0.4 MPa $m^{1/2}$
Subcritical tensile crack growth parameter, n_a	2
Subcritical shear crack growth threshold, K_{IIsc}	0.5 MPa $m^{1/2}$
Subcritical shear crack growth parameter, n_l	10

The remaining fracturing parameters adopted are also listed in Table 1.

Fig. 4 compares the simulated stress–strain and strain–time curves of granite when $\sigma_3 = 5$ MPa, $\sigma_2 = 50$ MPa, and $\sigma_1 = 278$ MPa, which lasted about 120 h. According to the elastic compression stage, the elastic modulus is $E = 54{,}000$ MPa, and the Poisson's ratio is $\nu = 0.4$. The initial crack radius in this granite sample is $l_0 = 1.05 \times 10^{-3}$ m. After entering the time-dependent loading stage, the subcritical propagation parameters for tensile and shear cracks are $A_a = 5.12 \times 10^{-5}$ m/h and $A_l = 3.45 \times 10^{-19}$ m/h. The remaining fracturing parameters adopted are also listed in Table 1.

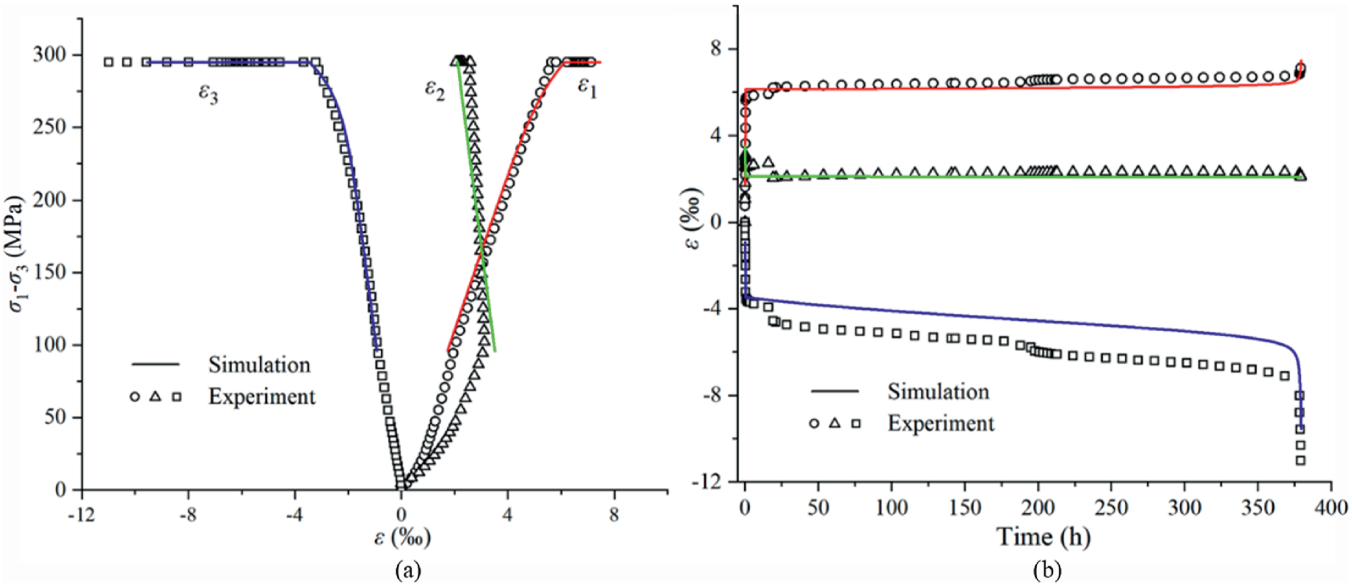

Fig. 3. Comparison between simulated and creep experimental results for granite when $\sigma_3 = 5$ MPa, $\sigma_2 = 100$ MPa, and $\sigma_1 = 300$ MPa: (a) Stress–strain curves; and (b) Strain–time curves.

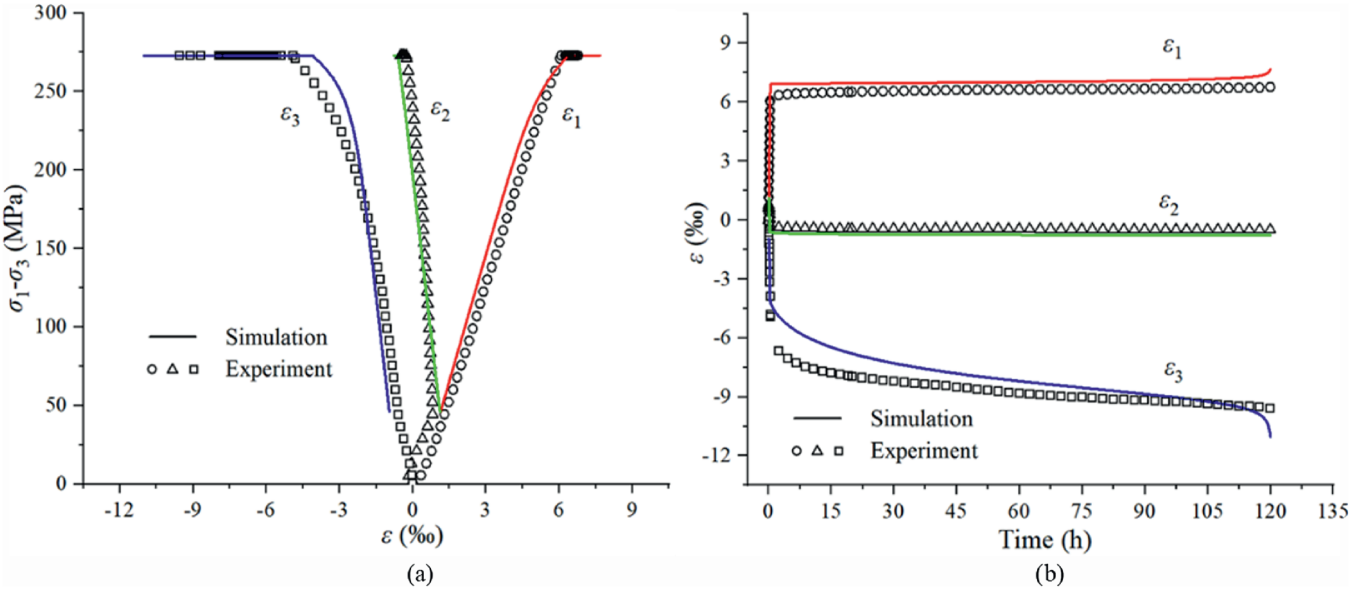

Fig. 4. Comparison between simulated and creep experimental results for granite when $\sigma_3 = 5$ MPa, $\sigma_2 = 50$ MPa, and $\sigma_1 = 278$ MPa: (a) Stress–strain curves; and (b) Strain–time curves.

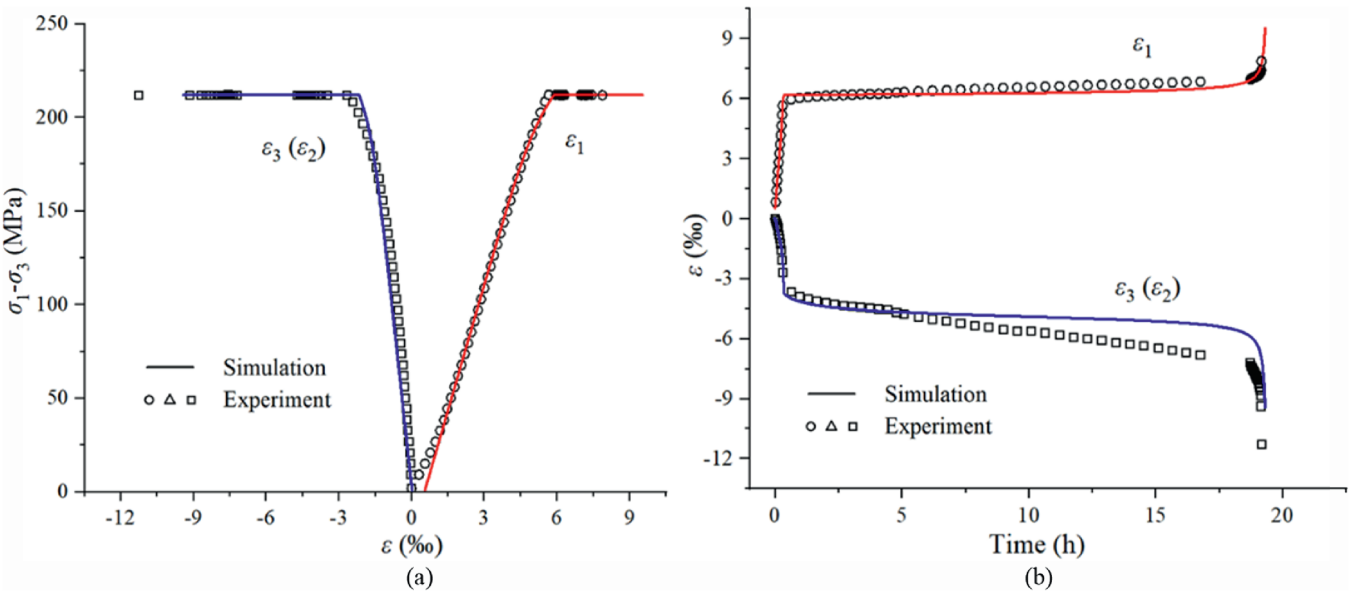

Fig. 5. Comparison between simulated and creep experimental results for granite when $\sigma_3 = 5$ MPa, $\sigma_2 = 5$ MPa, and $\sigma_1 = 217$ MPa: (a) Stress–strain curves; and (b) Strain–time curves.

Fig. 5 compares the simulated stress–strain and strain–time curves of granite when $\sigma_3 = 5$ MPa, $\sigma_2 = 5$ MPa, and $\sigma_1 = 217$ MPa, which lasted about 19 h. According to the elastic compression stage, the elastic modulus is $E = 45{,}000$ MPa, and the Poisson's ratio is $\nu = 0.38$. The initial crack radius in this granite sample is $l_0 = 1.15 \times 10^{-3}$ m. After entering the time-dependent loading stage, the subcritical propagation parameters for tensile cracks and shear cracks are $A_a = 1.76 \times 10^{-3}$ m/h and $A_l = 1.18 \times 10^{-15}$ m/h. The remaining fracturing parameters adopted are also listed in Table 1.

Given the presence of the unpredictable initial microcrack closure stage, the associated deformation is directly incorporated into the simulation results to facilitate an appropriate comparison with experimental data. For the granite under $\sigma_3 = 5$ MPa, $\sigma_2 = 100$ MPa, and $\sigma_1 = 300$ MPa, a sudden small increase in deformation was observed at about 16 h during the creep test, which was attributed to local fractures. Nonetheless, the simulation results showed good agreement with the experimental data, both during the instantaneous and the time-dependent loading processes. This indicates that the developed model could effectively capture the stress-induced anisotropic fracturing process under true triaxial stress.

4.3. Parameter sensitivity analysis

During the time-dependent loading stage, the subcritical growth parameters A_a and A_l for open-tensile and penetrative-shear cracks, respectively, are critical to the simulation results. Therefore,

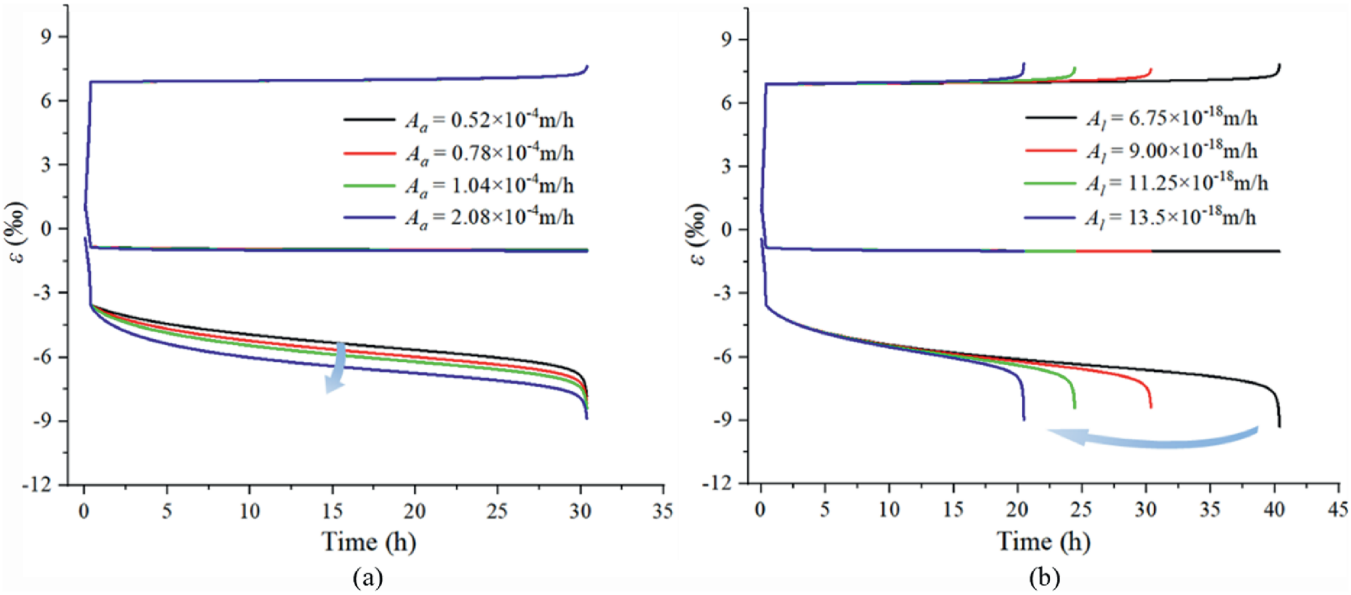

Fig. 6. Parameter sensitivity analysis for subcritical crack propagation parameters (a) A_a and (b) A_l under $\sigma_3 = 5$ MPa, $\sigma_2 = 30$ MPa, and $\sigma_1 = 259$ MPa.

sensitivity analysis was conducted for these two parameters to explore their influence under $\sigma_3 = 5$ MPa, $\sigma_2 = 30$ MPa, and $\sigma_1 = 259$ MPa. As shown in Fig. 6a, it can be found that the parameter A_a primarily affects the lateral dilatancy over time. A higher A_a leads to greater time-dependent lateral deformation, especially in the σ_3-direction under true triaxial stress. During the time-dependent loading stage, high σ_1 continuously generates microcracks oriented in a direction parallel to σ_1, which is reflected by the parameter A_a in this developed model. Additionally, the influence of parameter A_a on the time-dependent deformation in the σ_3-direction is significantly greater than that in the σ_2-direction. This is also consistent with the experimental observations, since crack propagation is inhibited in the σ_2-direction under true triaxial stress. As for the parameter A_l for penetrative-shear cracks, it primarily affects the failure time. A larger A_l would lead to a reduction in failure time. This also indicates that the penetrative-shear cracks are one key factor in controlling the time-dependent rock failure.

5. Discussion

The time-dependent failure of hard rock refers to the slow failure process of hard rock over time at a stress level below its strength. The essence of this behavior is also attributed to the evolution of internal cracks. On the basis of CAFM, the time effect could be introduced to describe the evolution of microcrack ensembles in the time-dependent failure process. In addition, it is worth noting that the failure process of hard rock is also a function of loading history. Different loading histories would result in different fracturing states in hard rock, significantly impacting subsequent deformation and fracturing behavior. If the pre-existing fracturing state of hard rock is ignored, it will inevitably lead to inaccurate analysis and prediction of the time-dependent failure process. In the failure process of hard rock, the propagation of microcracks remains the fundamental mechanism, whether driven by instantaneous or time-dependent loading. Although the complete loading–fracturing process could be divided into different loading stages (e.g. instantaneous loading stage, time-dependent loading stage, and others), the propagation of internal microcrack ensembles is continuous throughout the entire rock failure process. Later crack propagation must depend on the inner crack state at the previous moment. Therefore, it is convenient and effective to analyze the entire failure process of hard rock using the evolution of internal microcrack ensembles as the fundamental principle. Although this article only considers the time effect on the rock failure process, this approach is also effective for assessing the impact of other factors on hard rock, such as disturbances, heat, and water.

5.1. Anisotropic time-dependent crack propagation

Under true triaxial stress, the deviation between strains ε_2 and ε_3 becomes larger as the intermediate principal stress σ_2 increases, regardless of whether during the instantaneous or the time-dependent loading stage. This phenomenon is caused by the difference in stress-induced crack propagation abilities in σ_2-and σ_3-directions, referred to as anisotropic fracturing (Feng et al., 2019b). In order to analyze the time effect on the rock failure process under high triaxial stress, the time-dependent fracturing process of granite under $\sigma_3 = 5$ MPa, $\sigma_2 = 100$ MPa, and $\sigma_1 = 300$ MPa is taken as an example. As shown in Fig. 7, before entering the time-dependent loading stage, significant irreversible damage has already occurred in hard rock due to instantaneous loading. Under high stress, microcracks continue to propagate over time. No matter for tensile or shear cracks, the internal fracturing state in hard rock always shows significant anisotropy under true triaxial stress during the time-dependent loading stage, as depicted in Fig. 8. Fig. 9 shows the length increase of open-tensile and penetrative-shear cracks in different orientations. It could be observed that the time effect could not eliminate the anisotropy during the fracturing process of hard rock, and crack propagation is highly orientation-dependent under true triaxial stress during the time-dependent loading stage. Especially for penetrative-shear cracks, the time-dependent increase of cracks in critical orientations is extremely significant.

In the time-dependent failure process of hard rock, the time-dependent propagation rate of microcracks in different orientations is one key element. Figs. 10 and 11 show the crack propagation rates in different orientations at different times during the time-dependent loading stage. It could be observed that the time-dependent growth rate of cracks in different orientations exhibits

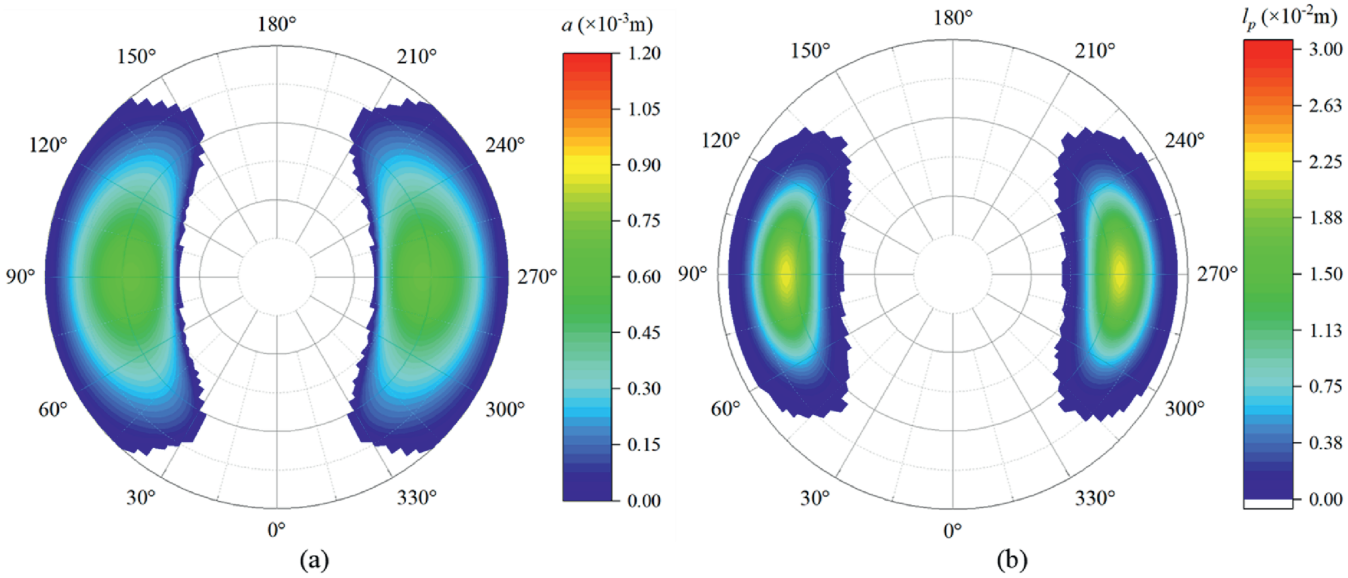

Fig. 7. Fracturing state in different orientations at the end of instantaneous loading: (a) Open-tensile cracks; and (b) Penetrative-shear cracks.

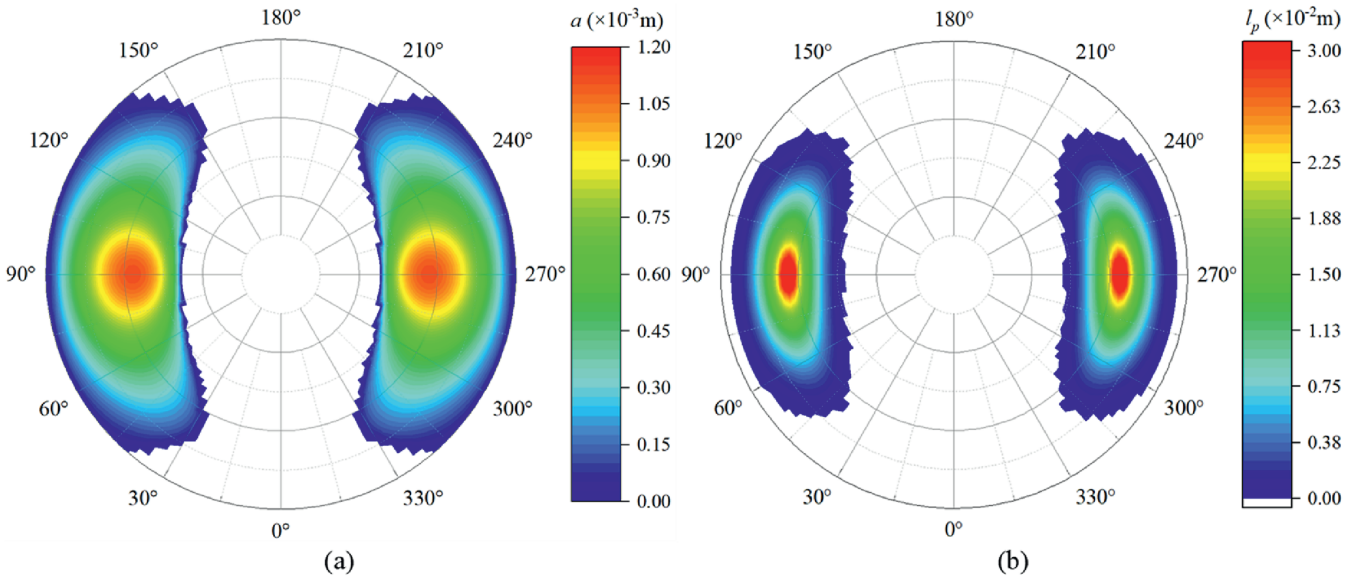

Fig. 8. Fracturing state in different orientations at 375 h during the time-dependent loading: (a) Open-tensile cracks; and (b) Penetrative-shear cracks.

significant anisotropic characteristics. At 5 h, 125 h, 250 h, and 375 h, the time-dependent propagation rates of open-tensile cracks near ($\theta = 58°$, $\varphi = 90°$) and ($\theta = 58°$, $\varphi = 270°$) are significantly higher than those in other orientations throughout the time-dependent loading stage. With the loading time, the propagation rates for open-tensile crack propagation significantly decrease. For penetrative-shear cracks, the time-dependent propagation rates of cracks near ($\theta = 64°$, $\varphi = 90°$) and ($\theta = 64°$, $\varphi = 270°$) are always greater than those in other orientations, and this trend will become more pronounced over time. In general, the time-dependent failure process of hard rock is still a competition for propagation among internal cracks with different orientations.

In order to further analyze the dependence of crack propagation rates on orientation, a comparative analysis was conducted on the crack propagation rates in several specific orientations, as shown in Figs. 12 and 13. Fig. 12 presents the variation of crack propagation rates at $\theta = 48°$, $56°$, $64°$, $70°$, and $78°$ when the dip $\varphi = 90°$. From Fig. 12a, it could be found that the propagation rates of tensile cracks gradually decrease over time. The time-dependent propagation rates of open-tensile cracks also vary significantly with the dip angle θ under a constant dip φ. As the dip angle θ increases, the time-dependent propagation rate of open-tensile cracks reaches its maximum near 58° at different time points during the creep loading stage and then rapidly decreases with the increase of θ. As shown in Fig. 12b, the time-dependent propagation rates of penetrative-shear cracks continue to increase over time. Under the same dip φ, the propagation rate of penetrative-shear cracks also increases in the dip range of 48°–64° and decreases in the dip range of 64°–78°. Generally, there are significant differences in the growth rates of microcracks in different orientations, which results in the time-dependent anisotropic failure process of hard rock under true triaxial stress.

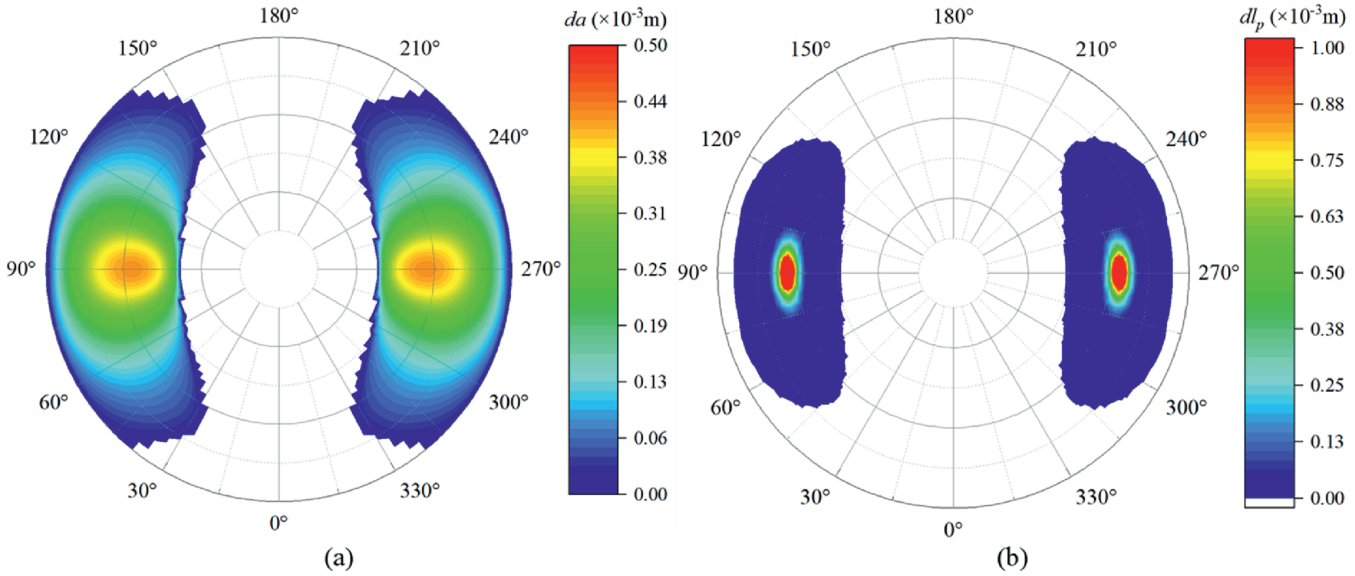

Fig. 9. Crack radius increment in different orientations from 0 h to 375 h: (a) Open-tensile cracks; and (b) Penetrative-shear cracks.

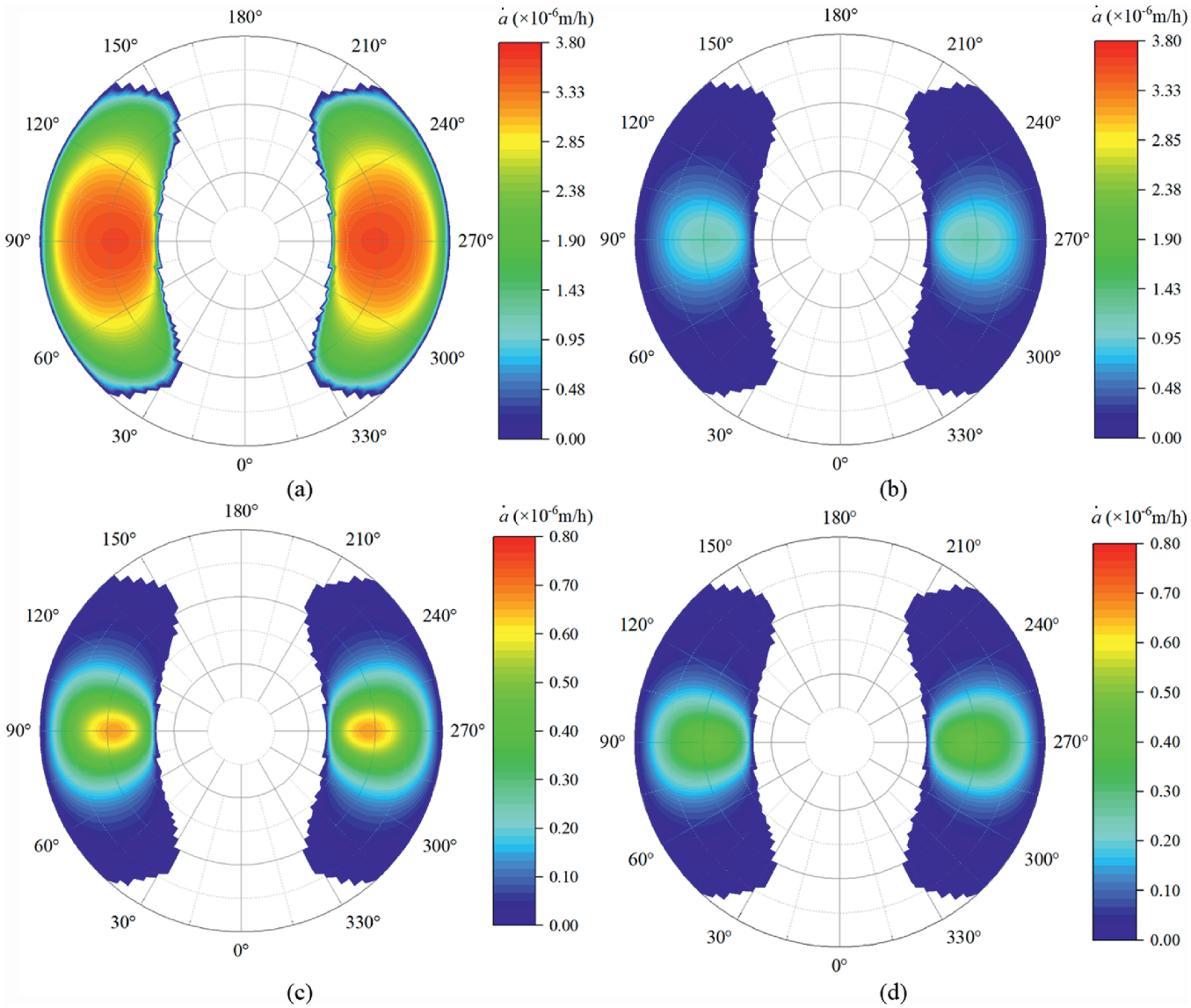

Fig. 10. Evolution of tensile crack growth rate with time in different orientations: (a) 5 h; (b) 125 h; (c) 250 h; and (d) 375 h.

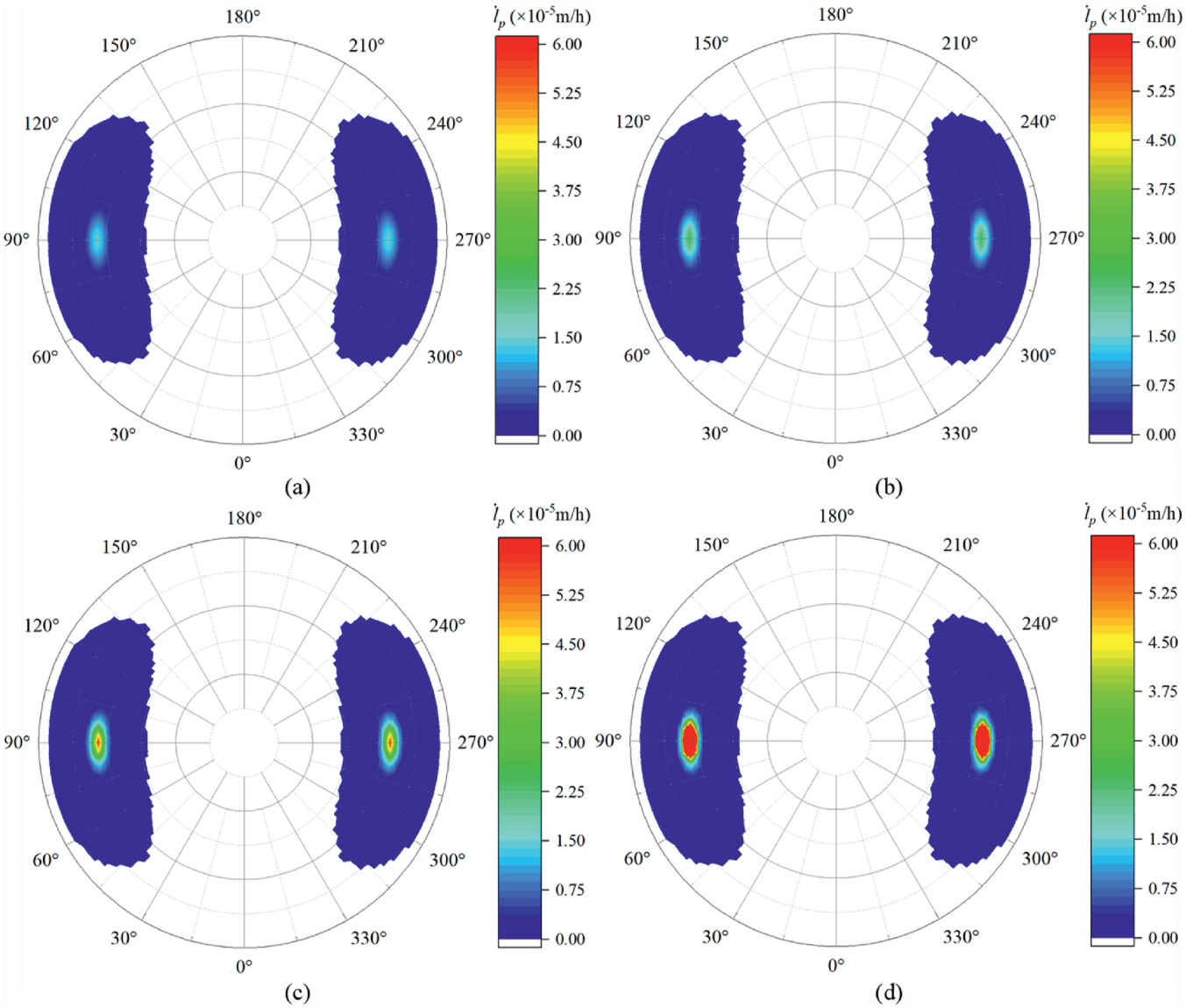

Fig. 11. Evolution of penetrative-shear crack growth rate with time in different orientations: (a) 5 h; (b) 125 h; (c) 250 h; and (d) 375 h.

Fig. 13 shows the variation of time-dependent crack propagation rate at $\varphi = 54°$, 63°, 72°, 81°, and 90° when the dip angle $\theta = 64°$. From Fig. 13a, it could be observed that the decreasing trend of time-dependent propagation rates of open-tensile cracks gradually slows down from $\varphi = 54°$ to $\varphi = 90°$ under the same θ. Meanwhile, as shown in Fig. 13b, the time-dependent propagation rate of penetrative-shear cracks shows a significant increasing trend with φ in the range of 54°–90° under the same θ. The above results demonstrate a significant variation in the time-dependent crack propagation rate in hard rock under true triaxial stress, which induces the time-dependent anisotropic failure of hard rock. In addition, the variation in time-dependent propagation rates indicates that the orientations near (64°, 90°) are still the concentrated area for penetrative-shear crack propagation, which has not been changed under the time effect and is consistent with the orientation of the microscopic fracturing plane in creep tests.

5.2. Evolution of time-dependent fracturing

In the process of model development, we did not adopt the traditional partition method for the time-dependent failure process of hard rock, which divides the rock failure process into decelerating creep, steady creep, and accelerating creep. This partition method is based on the deformation characteristics, but fails to provide a satisfactory mechanical explanation for the occurrence of these three creep stages. Hence, according to the fracturing characteristics, we divided the creep failure process from the perspective of the rock fracturing process, namely the stage dominated by time-dependent tensile fracturing and the stage dominated by time-dependent penetrative-shear fracturing. In the former stage, the tensile crack propagation rates show a significant decreasing trend with time. The decelerating creep stage could be primarily attributed to the decrease in the tensile crack propagation rates. In this stage, although the propagation rates of penetrative-shear cracks increase over time, the penetrative-shear cracks newly growing in the creep loading stage are not sufficient, and the inelastic deformation caused by crack coalescence is still dominated by the cracks generated in the instantaneous loading stage. As for the accelerating stage, the time-dependent penetrative-shear cracks have been fully

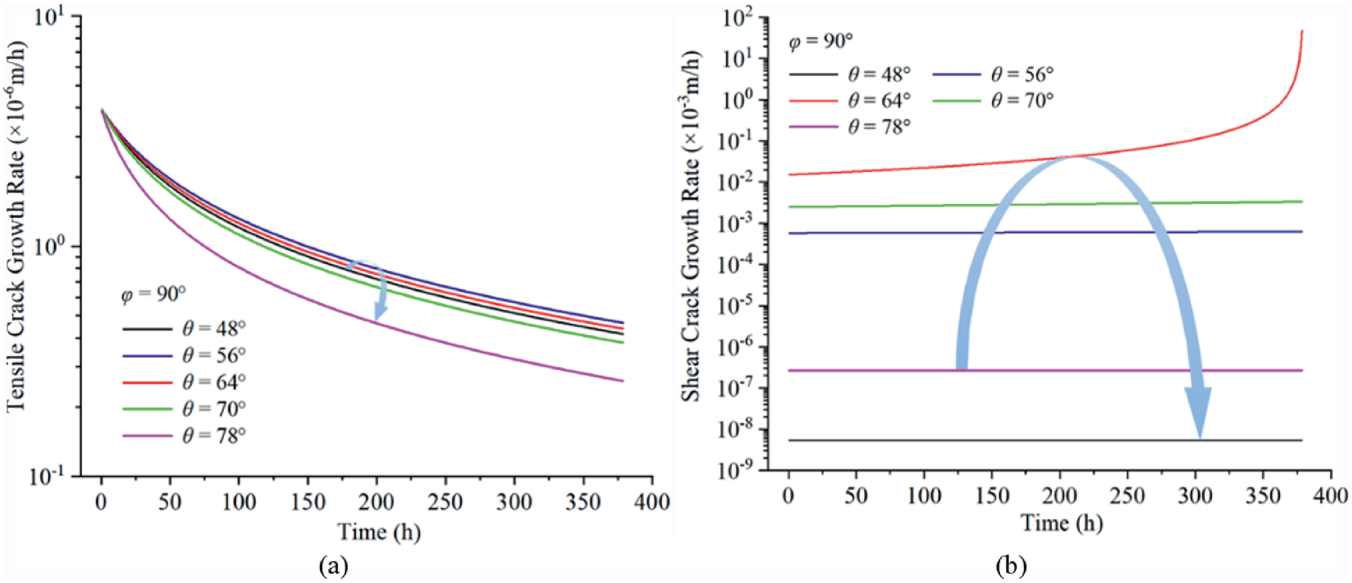

Fig. 12. Variation in time-dependent propagation rate with different dip angle θ over time: (a) Open-tensile cracks; and (b) Penetrative-shear cracks.

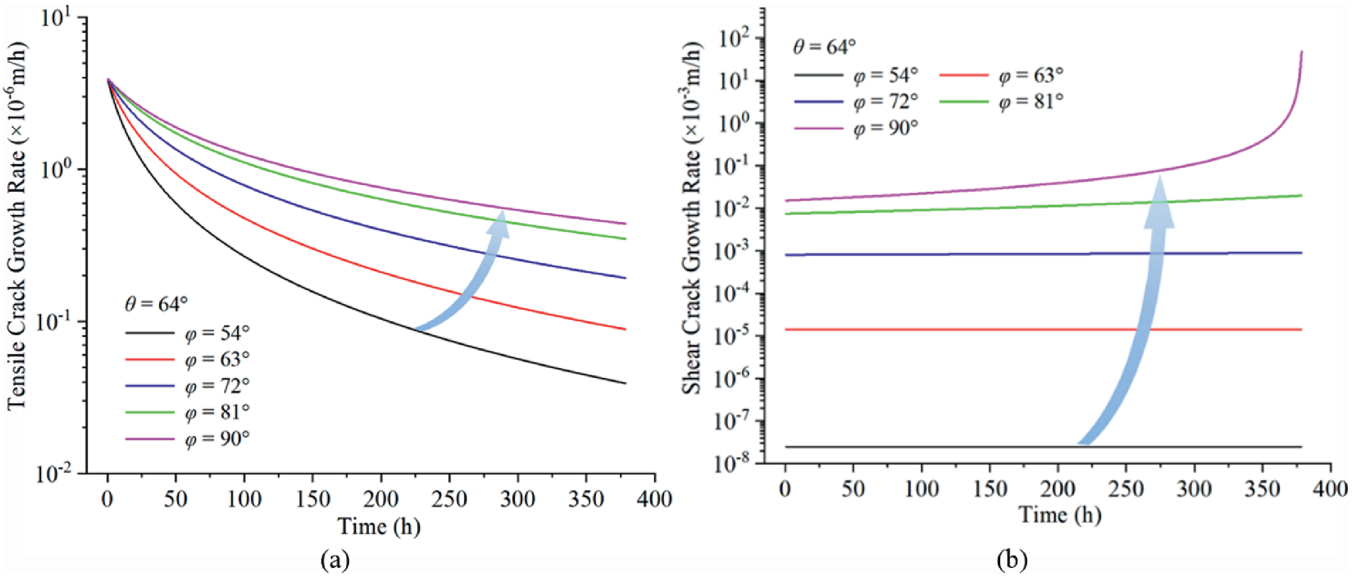

Fig. 13. Variation in time-dependent propagation rate with different dip φ over time: (a) Open-tensile cracks; and (b) Penetrative-shear cracks.

developed at this time, while the time-dependent tensile cracks gradually stop developing. As the time-dependent penetrative-shear cracks grow rapidly in critical orientations, the trend of crack coalescence becomes more pronounced. Thus, the accelerating creep stage is primarily attributed to the propagation of time-dependent penetrative-shear cracks in critical orientations. As for the steady creep stage, it should be regarded as a transitional stage, shifting from the stage dominated by open-tensile fracturing to the stage dominated by penetrative-shear fracturing. In this transitional stage, the time-dependent propagation rates of open-tensile cracks have greatly decreased, resulting in a limited increase in macroscopic deformation. At the same time, penetrative-shear cracks still develop stably at a relatively low propagation rate, without causing substantial crack coalescence. This dynamic evolution of microcracks results in the steady creep stage observed in macroscopic deformation during the time-dependent failure process, corresponding to the quiescence period in the acoustic emission (AE) monitoring results. Fig. 14 depicts the comparison between the macroscopic deformation and the average microcrack evolution tendency during the time-dependent loading stage. In the earlier time-dependent loading stage, the propagation of time-dependent open-tensile cracks dominates, while the fracturing process in the later time-dependent loading stage is primarily driven by the propagation of time-dependent penetrative-shear cracks. This process is generally consistent with the AE tendency monitored in creep tests (Zhao et al., 2021).

5.3. Preferred orientation of macroscopic failure plane

The time-dependent rock failure process could also be regarded as a competition for propagation among cracks with different

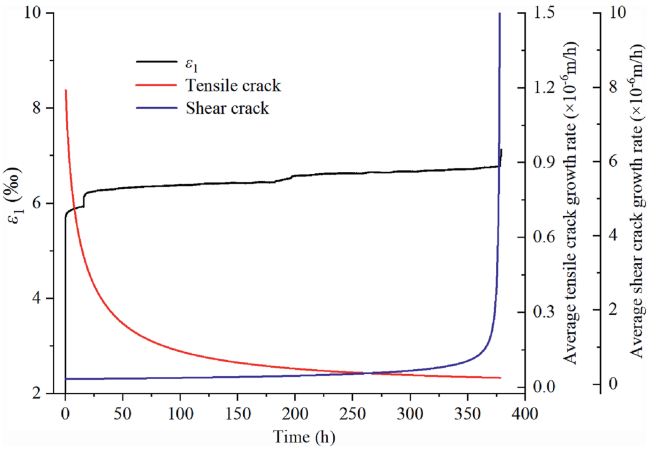

Fig. 14. Comparison between the macroscopic deformation and microcrack evolution during the time-dependent loading stage.

orientations. Compared to open-tensile cracks, penetrative-shear cracks play a critical role in connecting scattered cracks, significantly damaging the load-bearing structure. Therefore, in the developed model, the orientation where penetrative-shear cracks grow most rapidly is considered the preferred orientation for the macroscopic failure plane. As shown in Fig. 15, the orientations near (64°, 90°) are the concentrated area for the penetrative-shear crack propagation during the time-dependent loading stage, which is also close to the macroscopic failure plane orientation in tests. By comparing the dominant orientation of crack propagation in the instantaneous loading stage with that in the time-dependent loading stage, it is found that the time effect does not change the dominant orientation of crack propagation. This implies that the orientation of macroscopic failure plane under time-dependent loading is similar to that under instantaneous loading, which has been validated by experiments (Zhao et al., 2021).

5.4. Model analysis

Compared with other creep models, this developed model discards the conventional tri-modal partition method based on time-dependent deformation and instead adopts an analytical framework centred on time-dependent tensile and shear fracturing. This model successfully bridges the irreversible fracturing processes of hard rock during the instantaneous and the time-dependent loading stages. By focusing on the continuous crack propagation process, this model provides mechanistic insights into some key fracturing characteristics, such as macroscopic anisotropic time-dependent deformation and the similar macroscopic fracture plane orientation in instantaneous and time-dependent rock failure. Nonetheless, there are still several aspects that can be further refined for the model.

In the developed model, a complete decoupling method was adopted to address the interaction between cracks. The model assumes that each crack is situated in an undamaged rock matrix, thereby neglecting interactions between crack growths. However, considering the stress field superposition from interacting microcracks, this assumption would gradually deviate from reality as cracks coalesce. Therefore, for a more precise simulation, this model could be further optimized by incorporating crack interaction using methods such as the self-consistent method (Budiansky, 1965) or the Mori-Tanaka method (Benveniste, 1986).

Additionally, the time-dependent failure process of hard rock was attributed to subcritical crack growth. In the developed model, a power-law form was adopted to describe the subcritical crack growth rate, which is primarily based on data fitting from previous experiments. However, experimental schemes to observe subcritical crack propagation (e.g. double torsion tests and the short beam compression tests) are not conducted under true triaxial stress conditions. Although theoretical research suggests that the simplest power-law form yields good agreement with experimental data among various possible functional forms (Bernabé and Pec, 2022), further verification is still needed to

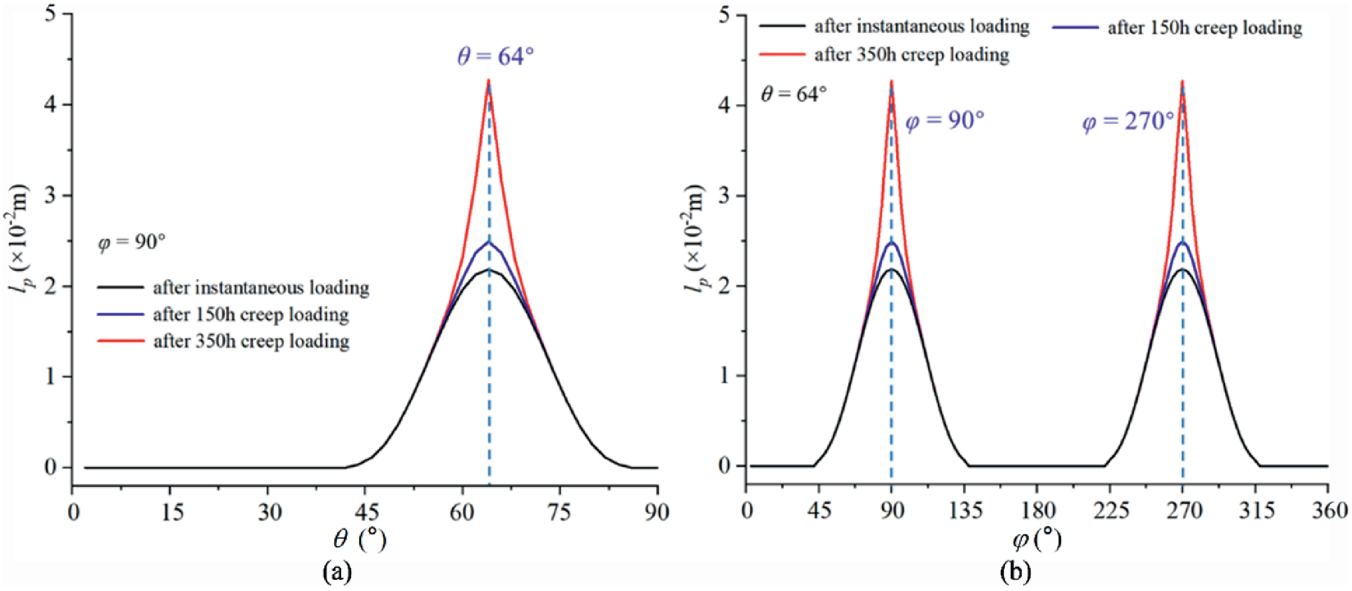

Fig. 15. Critical orientation of crack propagation of granite in instantaneous loading and time-dependent loading when $\sigma_3 = 5$ MPa, $\sigma_2 = 100$ MPa, and $\sigma_1 = 300$ MPa: (a) Critical dip angle θ; and (b) Critical dip φ.

determine its applicability under true triaxial stress conditions. If a more scientific subcritical crack growth model is obtained, the power-law form model used in this model could be directly replaced, without affecting the effectiveness of the theoretical framework. Given the scarcity of reports on subcritical crack propagation under true triaxial conditions, further investigation in this area remains necessary.

Furthermore, the developed model is based on the assumption of initial isotropy. However, the fracturing process of hard rock is a systematic problem involving multiple intertwined factors, and inelastic deformation reflects the comprehensive effects of these factors. For the geometrically anisotropic hard rocks (e.g. slate and gneiss), the mechanical properties and fracturing process vary with the combination of stress direction and rock foliations. Thus, when analyzing the progressive fracturing process of geometrically anisotropic rocks, the influence of rock inhomogeneity on crack propagation requires further investigation.

6. Conclusions

In this paper, a 3D time-dependent fracturing model is formulated to characterize the time-dependent failure process of hard rock under triaxial stress. This model discards the conventional tri-modal partition method based on time-dependent deformation and instead adopts an analytical framework centred on time-dependent tensile and shear fracturing. By focusing on the crack propagation process, this model successfully bridges the irreversible fracturing processes of hard rock during both the instantaneous and the time-dependent loading stages. The simulation results are in good agreement with experimental data. The findings reveal that the progressive failure of hard rock is attributed to the continuous accumulation of internal fracturing states, and the rock damage incurred during the instantaneous loading stage cannot be ignored. During the time-dependent loading stage, the crack propagation ability varies significantly with orientation under true triaxial stress, resulting in macroscopic anisotropic time-dependent deformation. Furthermore, this model provides mechanistic insights into some key fracturing characteristics, such as the similar orientation of macroscopic fracture planes in instantaneous and time-dependent rock failure. Generally, this developed 3D time-dependent fracturing model offers a novel perspective for understanding the time-dependent failure process of hard rock, which is beneficial for elucidating the evolution mechanism of time-delayed surrounding rock failure in deep engineering.

CRediT authorship contribution statement

Chen Fan: Methodology, Data curation, Writing – original draft, Formal analysis, Investigation. **Xia-Ting Feng:** Supervision, Writing – review & editing, Methodology. **Jun Zhao:** Supervision, Validation, Writing – review & editing, Funding acquisition. **Chengxiang Yang:** Supervision, Validation, Writing – review & editing. **Mengfei Jiang:** Supervision, Validation, Writing – review & editing.

Declaration of competing interest

The authors declare that they have no known competing financial interests or personal relationships that could have appeared to influence the work reported in this paper.

The author Xia-Ting Feng is the Editor-in-Chief for this journal and was not involved in the editorial review or the decision to publish this article.

Acknowledgements

The authors gratefully acknowledge the financial support from the National Natural Science Foundation of China (Grant No. 52209125). We are also particularly grateful for the kind assistance provided by Ms. Xinyue Wang.

References

Anderson, O.L., Grew, P.C., 1977. Corrosion theory of crack propagation with applications to geophysics. Rev. Geophys. 15, 77–104.
Atkinson, B.K., 1987. Fracture Mechanics of Rock. Academic Press, London, UK.
Becker, T.H., Marrow, T.J., Tait, R.B., 2011. An evolution of the double torsion technique. Exp. Mech. 51 (9), 1511–1526.
Benveniste, Y., 1986. On the Mori-Tanaka method in cracked bodies. Mech. Res. Commun. 13, 193–201.
Bernabé, Y., Pec, M., 2022. Brittle creep and failure: a reformulation of the wing crack model. J. Geophys. Res. Solid Earth 127 e2022JB024610.
Bikong, C., Hoxba, D., Shao, J.F., 2015. A micro-macro model for time-dependent behavior of clayey rocks due to anisotropic propagation of microcracks. Int. J. Plast. 69, 73–88.
Brantut, N., Baud, M., Heap, M.J., Meredith, P.G., 2012. Micromechanics of brittle creep in rocks. J. Geophys. Res. 117, B08412.
Budiansky, B., 1965. On the elastic moduli of some heterogeneous materials. J. Mech. Phys. Solid. 13, 233, 226.
Fan, C., Feng, X.T., Zhao, J., Yang, C.X., Jiang, M.F., 2025a. Meso-mechanical mechanism of ordered mica alignment on the progressive failure process of granite under different lateral stress directions. Int. J. Rock Mech. Min. Sci. 186, 106037.
Fan, C., Feng, X.T., Fu, L.J., Zhao, J., Yang, C.X., Yao, Z.B., Wang, J., Wei, F., 2023. Evolution law and mechanism of time-delayed spalling in as deep TBM tunnel: a case study. Eng. Geol. 325, 107309.
Fan, C., Feng, X.T., Zhao, J., Yang, C.X., Jiang, M.F., 2025b. Multiscale anisotropic fracturing model of hard rock based on the competitive process of crack propagation. J. Rock Mech. Geotech. Eng. 17 (8), 4952–4965.
Feng, X.T., Kong, R., Zhang, X.W., Yang, C.X., 2019b. Experimental study of failure differences in hard rock under true triaxial compression. Rock Mech. Rock Eng. 52, 2109–2122.
Feng, X.T., Xiao, Y.X., Feng, G.L., Yao, Z.B., Chen, B.R., Yang, C.X., Su, G.S., 2019a. Study on the development process of rockbursts. Chin. J. Rock Mech. Eng. 38 (4), 649–673 (in Chinese).
He, B.G., Wang, L., Feng, X.T., Zhen, R.L., 2023. Failure modes of jointed granite subjected to weak dynamic disturbance under true-triaxial compression. Rock Mech. Rock Eng. 56 (11), 7939–7957.
Horii, H., Nemat-Nasser, S., 1983. Overall moduli of solids with microcracks: load-induced anisotropy. J. Mech. Phys. Solid. 31 (2), 155–171.
Jiang, M.F., Feng, X.T., Zhao, J., Yang, C.X., Wang, G., Fan, C., 2024. Time-dependent failure characteristics of natural jointed granite of deep tunnel under different dip angles conditions. Acta Geotech. 19, 3075–3093.
Jiang, M.F., Xue, J.C., Zhao, J., 2025. Time to failure prediction and model of Beishan granite under true triaxial stresses. Mech. Time-Dependent Mater. 29, 3.
Ko, T.Y., Kemeny, J., 2011. Subcritical crack growth in rocks under shear loading. J. Geophys. Res. Solid Earth 116, B01407.
Kontogianni, V.A., Stiros, S.C., 2005. Induced deformation during tunnel excavation: evidence from geodetic monitoring. Eng. Geol. 79 (1), 115–126.
Krajcinovic, D., Fanella, D., 1986. A micromechanical damage model for concrete. Eng. Fract. Mech. 25, 585–596.
Li, X., Li, L., Qi, C., 2024. A true triaxial compression-induced microcracking model for evaluating short-term progressive and long-term creep failures of brittle rock. Int. J. Rock Mech. Min. Sci. 175, 105669.
Li, Z., Xiong, Z., Chen, H., Lu, H., Ma, C., Liu, Y., 2020. Analysis of stress-strain relationship of brittle rock containing microcracks under water pressure. Bull. Eng. Geol. Environ. 79, 1909–1918.
Okubo, S., Fukui, K., Hashiba, K., 2008. Development of a transparent triaxial cell and observation of rock deformation in compression and creep tests. Int. J. Rock Mech. Min. Sci. 45 (3), 351–361.
Ritchie, R.O., 1988. Mechanisms of fatigue crack propagation in metals, ceramics and composites: role of crack tip shielding. Mater. Sci. Eng.: A. 103 (1), 15–28.
Shao, J.F., Chau, K.T., Feng, X.T., 2006. Modeling of anisotropic damage and creep deformation in brittle rocks. Int. J. Rock Mech. Min. Sci. 43 (4), 582–592.
Shao, J.F., Zhu, Q.Z., Su, K., 2003. Modeling of creep in rock materials in terms of material degradation. Comput. Geotech. 30 (7), 549–555.
Sisodiya, M., Zhang, Y.D., 2022. A time-dependent directional damage theory for

brittle rocks considering the kinetics of microcrack growth. Rock Mech. Rock Eng. 55 (5), 2693–2710.
Tran-Manh, H., Sulem, J., Subrin, D., 2016. Progressive degradation of rock properties and time-dependent behavior of deep tunnels. Acta Geotech. 11 (3), 693–711.
Wei, Y., Chen, Q., Huang, H., Xue, X., 2021. Study on creep models and parameter inversion of columnar jointed basalt rock masses. Eng. Geol. 290, 106206.
Xu, T., Zhou, G.L., Heap, M.J., Yang, S.Q., Konietzky, H., Baud, P., 2018. The modeling of time-dependent deformation and fracturing of brittle rocks under varying confining and pore pressures. Rock Mech. Rock Eng. 51, 3241–3263.
Yang, L., Mei, J., Sheng, X., Yang, W., Li, J., 2021. Cracking and creep behavior of rocks considering propagation and interaction of adjacent cracks under hydro-mechanical coupling. Rock Mech. Rock Eng. 54, 4099–4110.
Yang, W.D., Zhang, Q.Y., Li, S.C., Wang, S.G., 2014. Time-dependent behavior of diabase and a nonlinear creep model. Rock Mech. Rock Eng. 47 (4), 1211–1224.
Zhao, J., Feng, X.T., Yang, C.X., Zhou, Y.Y., Zhang, Y., 2021. Study on time-dependent fracturing behaviour for three different hard rock under high true triaxial stress. Rock Mech. Rock Eng. 54 (3), 1239–1255.
Zhao, L.Y., Zhu, Q.Z., Xu, W.Y., Dai, F., Shao, J.F., 2016. A unified micromechanics-based damage model for instantaneous and time-dependent behaviors of brittle rocks. Int. J. Rock Mech. Min. Sci. 84, 187–196.
Zhao, Y.L., Wang, Y.X., Wang, W.J., Wan, W., Tang, J.Z., 2017. Modeling of non-linear rheological behavior of hard rock using triaxial rheological experiment. Int. J. Rock Mech. Min. Sci. 93, 66–75.

Prof. Xia-Ting Feng received his PhD degree at Northeastern University of Technology (now Northeastern University since 1993), China in 1992, and then took the position of lecturer, associate professor, and professor at the same university. He joined the Institute of Rock and Soil Mechanics, Chinese Academy of Sciences (CAS) in 1998 as a Professor of the Hundred Talent Program of the CAS and Deputy Director in Charge and Director during 2001–2005. He has worked as Director of the State Key Laboratory of Geomechanics and Geotechnical Engineering since 2007. He has worked at Northeastern University, China, as a Vice President since September 2017. In February 2021, he became president of Northeastern University. He is President of the Federation of International Geo-engineering Societies (FedIGS), President of the International Society for Rock Mechanics (ISRM) Commission on Design Methodology, member of the ISRM Commission on Testing Methods, and President of the Chinese Society for Rock Mechanics and Engineering (CSRME). He was the past President of ISRM from 2011 to 2015. He is also Editor-in-Chief of *Journal of Rock Mechanics and Geotechnical Engineering (JRMGE)*, and Associate Editor-in-Chief of *Chinese Journal of Theoretical and Applied Mechanics*. He is a member of the Editorial Board of *Rock Mechanics and Rock Engineering*. His research interests cover rock mechanics for deep rock engineering. He published more than 200 technical papers and the English books "*Rock Engineering Design*" and "*Rock Engineering Risk*" with Prof. John Hudson. He has edited five volumes of the book "*Rock Mechanics and Rock Engineering*" (CRC Press) and the book "*Rockburst*" (Elsevier).